J Arid Land (2018) 10(5): 781–793
https://doi.org/10.1007/s40333-018-0022-1

Science Press Springer-Verlag

Estimation of net primary productivity and its driving factors in the Ili River Valley, China

JIAO Wei[1,2], CHEN Yaning[1*], LI Weihong[1], ZHU Chenggang[1], LI Zhi[1]

[1] State Key Laboratory of Desert and Oasis Ecology, Xinjiang Institute of Ecology and Geography, Chinese Academy of Sciences, Urumqi 830011, China;
[2] School of Remote Sensing and Information Engineering, Wuhan University, Wuhan 430079, China

Abstract: Net primary productivity (NPP), as an important variable and ecological indicator in grassland ecosystems, can reflect environmental change and the carbon budget level. The Ili River Valley is a wetland nestled in the hinterland of the Eurasian continent, which responds sensitively to the global climate change. Understanding carbon budget and their responses to climate change in the ecosystem of Ili River Valley has a significant effect on the adaptability of future climate change and sustainable development. In this study, we calculated the NPP and analyzed its spatio-temporal pattern of the Ili River Valley during the period 2000–2014 using the normalized difference vegetation index (NDVI) and an improved Carnegie-Ames-Stanford (CASA) model. Results indicate that validation showed a good performance of CASA over the study region, with an overall coefficient of determination (R^2) of 0.65 and root mean square error (RMSE) of 20.86 g C/(m^2·a). Temporally, annual NPP of the Ili River Valley was 599.19 g C/(m^2·a) and showed a decreasing trend from 2000 to 2014, with an annual decrease rate of –3.51 g C/(m^2·a). However, the spatial variation was not consistent, in which 55.69% of the areas showed a decreasing tendency, 12.60% of the areas remained relatively stable and 31.71% appeared an increasing tendency. In addition, the decreasing trends in NPP were not continuous throughout the 15-year period, which was likely being caused by a shift in climate conditions. Precipitation was found to be the dominant climatic factor that controlled the inter-annual variability in NPP. Furthermore, the correlations between NPP and climate factors differed along the vertical zonal. In the medium-high altitudes of the Ili River Valley, the NPP was positively correlated to precipitation and negatively correlated to temperature and net radiation. In the low-altitude valley and high-altitude mountain areas, the NPP showed a negative correlation with precipitation and a weakly positive correlation with temperature and net radiation. The results suggested that the vegetation of the Ili River Valley degraded in recent years, and there was a more complex mechanism of local hydrothermal redistribution that controlled the growth of vegetation in this valley ecosystem.

Keywords: net primary productivity; Carnegie-Ames-Stanford model; spatio-temporal pattern; climatic impacts; precipitation; normalized difference vegetation index

Citation: JIAO Wei, CHEN Yaning, LI Weihong, ZHU Chenggang, LI Zhi. 2018. Estimation of net primary productivity and its driving factors in the Ili River Valley, China. Journal of Arid Land, 10(5): 781–793. https://doi.org/10.1007/s40333-018-0022-1

1 Introduction

Net primary productivity (NPP) is a reflection of the production and carbon (C) sink capacity of

*Corresponding author: CHEN Yaning (E-mail: chenyn@ms.xjb.ac.cn)
Received 2017-05-31; revised 2018-06-04; accepted 2018-06-12

an ecosystem and is recognized as a key topic in ecology (Pan et al., 2015; Li et al., 2016). With the development of global change research, the estimation of vegetation NPP has attracted increased attention from scholars. In fact, vegetation NPP has become an indispensable index and the core content in the study of the effects of climate change on terrestrial ecosystems (Li et al., 2011; Li et al., 2016). It has even become an important index to assess national grain security (He et al., 2017). Scholars use a variety of methods to estimate vegetation NPP in different regions of the world as well as to analyze vegetation NPP from different angles (Liang et al., 2015). Recent findings from numerous studies suggest that vegetation NPP has experienced slight increases around the world due to global warming and the fertilizer utilization (Piao et al., 2011; Zhang et al., 2013; Li et al., 2016). Some scholars also assert that the phenomenon of vegetation degradation has appeared in parts of drought and cold regions under the impacts of changing climate and human activities (Zhao et al., 2010). However, the response of vegetation NPP in regions of complex terrain to changing climate is not yet well known.

Grassland is the largest terrestrial ecosystem in the world. Moreover, it is highly sensitive and vulnerable to climate change (e.g., it can respond by experiencing prolonged growth periods), which makes it a preferred study subject for investigating global changes (Zhang et al., 2008; Fan et al., 2012; Mu et al., 2013; Zhou et al., 2014). Within the realm of grassland ecology, a long-term quantitative survey of grassland biomass and dynamic monitoring of vegetation NPP could provide a strong support for evaluating the productivity of grassland ecosystems and also help to realize the sustainable development of grassland ecosystems (Wang et al., 2011). With recent developments in the study of vegetation NPP in grassland ecosystems, the estimation model of NPP has become more mature, from traditional estimation method (including actual-measurement method, climate related statistical model and the ecological process model) to the light energy utilization model based on remote sensing technology (Gang et al., 2015; Liang et al., 2015). At present, some researchers used the light energy utilization model to estimate vegetation NPP, which makes it possible to obtain real-time observation data at a large scale (Liang et al., 2015; Cui et al., 2018). Carnegie-Ames-Stanford (CASA), which is a representative model based on remote sensing data, can estimate vegetation NPP at different scales. And its accuracy has been verified in several studies (Zhu et al., 2005).

The Ili River Valley, which is located in the western border of China, is a wetland nestled in the hinterland of the Eurasian continent. A grassland ecosystem dominates the main portion of the valley, covering an area of 3.4×10^6 hm^2. This region is an important production base for agriculture and animal husbandry of Xinjiang. The responsible use of grassland resources and the sustainable development of the ecological environment both play important roles in promoting the target of "Belt and Road Initiatives" and in maintaining local socioeconomic stability. In recent years, research focusing on the ecological environment of the Ili River Valley has been intensified (Chen et al., 2010; Zhang et al., 2012), with most studies investigating the vegetation index (Yan et al., 2013; Chen et al., 2016), soil and water conservation in the hillside (Chen et al., 2012; Li et al., 2016), and the physical and chemical characteristics of the soil (Sun et al., 2016; Zhou et al., 2016). While all of these studies laid a solid foundation for further explorations of the changing characteristics and sustainable development of the ecological environment in valley, research on the changing characteristics of grassland ecosystems from the perspective of NPP is still lacking.

In order to accurately reflect the temporal and spatial pattern of vegetation NPP in the Ili River Valley, we used the MODIS NDVI and meteorological station data during the period 2000–2014, combined with a remote sensing-based carbon model (i.e., CASA) and measured data to estimate vegetation NPP. Meanwhile, correlation between NPP and major climate factors were analyzed. The findings can provide a scientific basis for restoration and the sustainable utilization of grassland ecosystems in this region.

2 Materials and methods

2.1 Study area

The Ili River Valley (42°14′16″–45°50′30″N, 80°09′42″–84°56′50″E), located in the western

Tianshan Mountains of China, belongs to the hinterland of the Eurasian continent. The region is a depression basin approximately 55.3×10^3 km^2 that serves as a separation zone between the northern and southern Tianshan Mountains. The basin features a typical temperate continental climate, with precipitation gradually increasing from west to east. The annual mean temperature is 10.4°C and annual sunshine is approximately 2898.4 h (Sun et al., 2010; Yang et al., 2010). Annual precipitation in the basin is around 417.6 mm, which makes the area rich in waterpower and natural grassland resources. The valley area of the basin is also known for its well-established agricultural and animal husbandry industries.

2.2 Data sources and pretreatment

2.2.1 Data

The MODIS datasets used in the model were derived from National Aeronautics and Space Administration (NASA) series satellites. Specifically, data of 1-km resolution MOD13 (NDVI) and MOD12 (land use and land cover data) were used (https://ladsweb.nascom.nasa.gov/data/order.html). The MODIS NDVI dataset was the 16-day composite of daily remotely sensed data with a data range from 2000 to 2014. The data range for the MOD12 dataset is from 2000 to 2014 and the time resolution was one year. The topography information of this region was obtained from the United States Geological Survey (USGS)-produced digital elevation model (DEM), with a 90-km resolution.

Daily meteorological data recorded from 9 meteorological stations across the Ili River Valley during the period 2000–2014 were obtained from the Climate Database of the China Meteorological Administration (http://cdc.cma.gov.cn/home.do). The data include daily precipitation, temperature, wind velocity, vapor pressure, relative humidity, sunshine percentage, relative humidity, and daily order.

2.2.2 Data pretreatment

To begin the process of pretreatment, we used the MODIS Reprojection Tool (MRT) to splice, project and format the conversions. We converted the images from HDF to Tiff formats, and configured the coordinate system to WGS84/Geographic. The maximum value composite (MVC) method was used to reduce the noise (i.e., disturbance from clouds, atmosphere, and changes in solar altitude angles) in NDVI data and to generate a monthly NDVI series. We clipped the images according to the boundary map, and the ArcGIS10.2 converted DN values into standard ones.

We generated the gridded meteorological data (at 0.01°×0.01° spatial resolution), which included air temperature, precipitation, wind velocity, vapor pressure, relative humidity, sunshine percentage and relative humidity, from meteorological stations across the Ili River Valley based on the Kriging interpolation technique. The processed NDVI and land cover data were further resampled to a 0.01°×0.01° spatial resolution. In addition, the DEM data were used to revise the temperature data.

2.3 Methods

2.3.1 NPP algorithm

We used the CASA model to estimate NPP as a product of the amount of absorbed photosynthetic active radiation (APAR, MJ/m^2) and light use efficiency (ε, g C/MJ) (Potter et al., 1993; Field et al., 1995). For a given geographic coordinate (x) at month t, NPP is calculated as:

$$\mathrm{NPP}(x,t)=\mathrm{APAR}(x,t)\times\varepsilon(x,t), \tag{1}$$

where t is the period that NPP is cumulated; and x is the pixel in a remote sensing image.

The two parameters are calculated as:

$$\mathrm{APAR}(x,t)=\mathrm{SOL}(x,t)\times\mathrm{FPAR}(x,t)\times0.5, \tag{2}$$

$$\varepsilon(x,t)=T_{\varepsilon1}(x,t)\times T_{\varepsilon2}(x,t)\times W_{\varepsilon}(x,t)\times\varepsilon_{\max}, \tag{3}$$

where $\mathrm{SOL}(x,t)$ is the surface total radiation (MJ/m^2); $\mathrm{FPAR}(x,t)$ is the absorption ratio of photosynthetic active radiation; $T_{\varepsilon1}(x,t)$ and $T_{\varepsilon2}(x,t)$ are the limiting effects of low temperature and high temperature on the utilization of light energy, respectively; $W_{\varepsilon}(x,t)$ is the water stress

coefficient; and ε_{max} is the maximum utilization of light energy under ideal condition (g C/MJ).

The relationship between FPAR and NDVI and simple ration (SR) has been near-linear in some studies (Hatfield et al., 1984; Ruimy and Saugier, 1994). Furthermore, the SR can be calculated by the NDVI (Eq. 6). The relationships between FPAR and NDVI and SR are given by:

$$\mathrm{FPAR}_{\mathrm{NDVI}}(x,t)=\frac{\mathrm{NDVI}(x,t)-\mathrm{NDVI}(i,\min)}{\mathrm{NDVI}(i,\max)-\mathrm{MDVI}(i,\min)}\times(\mathrm{FPAR}_{\max}-\mathrm{FPAR}_{\min})+\mathrm{FPAR}_{\min}, \quad (4)$$

$$\mathrm{FPAR}_{\mathrm{SR}}(x,t)=\frac{\mathrm{SR}(x,t)-\mathrm{SR}(i,\min)}{\mathrm{SR}(i,\max)-\mathrm{SR}(i,\min)}\times(\mathrm{FPAR}_{\max}-\mathrm{FPAR}_{\min})+\mathrm{FPAR}_{\min}, \quad (5)$$

$$\mathrm{SR}=\frac{1+\mathrm{NDVI}(x,t)}{1-\mathrm{NDVI}(x,t)}, \quad (6)$$

where FPAR_{min}=0.001, and FPAR_{max}=0.095. At the same time, the values of NDVI(i,min) and NDVI(i,max) correspond to 95% and 5% of the NDVI values of vegetation type i, respectively. The land cover-type-dependent NDVI values for 95% and 5% different vegetation populations are shown in Table 1. A comparison between the two indices indicates a large bias in the estimate of FPAR from NDVI and a small bias in the estimate of FPAR from SR, respectively. Based on the example of a previous study, we used the mean value as the FPAR (Zhu et al., 2006).

The calculation methods of some parameters in the model were improved. We calculated the SOL by using the experienced coefficient from Hou et al. (1993) and also introduced land use data to estimate the light energy utilization ratio of different vegetation types and to realize parameter localization. The maximum utilization of light energy (ε_{max}) is shown in Table 2. These data come from a previous study (Feng et al., 2014), which are calculated by the observed data. More details about the CASA model, including descriptions of calibration and data processing, can be found in Zhu et al. (2007).

Table 1 NDVI_{max}, NDVI_{min}, SR_{max} and SR_{min} of typical vegetation types in Northwest China

Code	Vegetation type	NDVI_{max}	NDVI_{min}	SR_{max}	SR_{min}
0	Water body	0.241	–0.300	1.635	0.538
1	Evergreen needle-leaf forest	0.757	0.143	7.230	1.334
2	Evergreen broadleaf forest	0.334	0.023	2.003	1.047
3	Deciduous needle-leaf forest	0.803	0.003	9.152	1.006
4	Deciduous broadleaf forest	0.872	0.083	14.625	1.181
5	Mixed forest	0.842	0.130	11.658	1.299
6	Closed shrub land	0.564	0.107	3.587	1.240
7	Opened shrub land	0.427	0.079	2.490	1.172
8	Multi-tree grassland	0.816	0.023	9.870	1.047
9	Savanna	0.788	0.011	8.434	1.022
10	Grassland	0.633	0.028	4.450	1.058
11	Permanent wetland	0.789	0.001	8.479	1.002
12	Farmland	0.763	0.133	7.439	1.307
13	City	0.653	0.077	4.764	1.167
14	Mixed land with crop and natural vegetation	0.838	0.227	11.346	1.587
15	Snow and ice	0.077	–0.056	1.167	0.894
16	Bare or poor vegetation cover land	0.134	0.037	1.309	1.077

Note: NDVI_{max} and NDVI_{min} indicate the maximum and minimum normalized difference vegetation indices, respectively. SR_{max} and SR_{min} indicate the maximum and minimum simple rations, respectively. Data are calculated from MODIS data by the MATLAB.

2.3.2 Sample collection of model verification

We used the actual value of vegetation NPP to verify the model. Based on changes in natural vegetation belt in the Ili River Valley, we uniformly arranged 18 quadrates and determined location information through GPS. Then, based on the representative principle, we randomly

selected 5 quadrates in each site at the length, width, and depth of 30 cm.

Table 2 Maximum light use efficiency (ε_{max}) of typical vegetation types

Land use type	ε_{max} (g C/MJ)	Land use type	ε_{max} (g C/MJ)
Forest	0.774	Wetland	0.357
Farmland	0.604	City	0.202
Grassland	0.380	Bare land	0.258
Water body	0.296	Shrub	0.380

Note: Data are referenced from Feng et al. (2014).

We proceeded to harvest and transport the aboveground vegetation from the quadrates and the plants were dried to calculate their weight in the laboratory. Next, we removed the underground roots from the soil and transported them to the lab. After rinsing them thoroughly with water, the roots were placed in an incubator for 48 h at a temperature of 70°C. Next, we tested their weight in the laboratory. According to previous studies, the coefficient of carbon conversion was 0.45 (Tang et al., 2014). Then, we calculated the value of NPP in the quadrates. Finally, based on latitude and longitude information of the sites, we spatially extracted and analyzed experimental and simulated data.

2.3.3 Trend and partial correlation analysis

(1) Trend analysis

To further discern the trend of annual NPP, we examined linear trend estimations on a per-pixel basis to establish a linear regression relationship between NPP and time. The method we chose for this process is Sen's slope. Additional details about this approach can be found in Wang et al. (2013). The slope is calculated as:

$$\beta = \text{Median}(\frac{x_j - x_i}{j - i}) \quad \forall j > i, \tag{7}$$

where β is the average change rate of this sequence (g C/(m^2•a)). Here, β>0 was considered an increasing trend and β<0 a decreasing one, while median is the median function.

(2) Stability analysis

In order to analyze the stability of NPP in the Ili River Valley, we used standard deviation to reflect the traits of volatility. Standard deviation is calculated as:

$$\text{Stdev} = \sqrt{\frac{1}{n}\sum_{i=1}^{n}(\text{NPP}_i - \overline{\text{NPP}})^2}, \tag{8}$$

where Stdev is the standard deviation; $\overline{\text{NPP}}$ is the annual NPP; and NPP$_i$ is the value of NPP at the i^{th} year. Using the natural fracture method, the vegetation NPP standard deviation was divided into the following five categories: higher volatility, high volatility, middle volatility, low volatility, and lower volatility, with the points of 29.95, 17.36, 10.89, 5.79, and 0.00, respectively. We then analyzed the stability of the vegetation NPP in the study area during the period 2000–2014.

(3) Correlation analysis

To further discern the correlations of annual NPP and driven factors, we calculated the correlation on a per-pixel basis to establish the relationship between variables and NPP.

$$R_{xy} = \frac{\sum_{i=1}^{n}((X_i - \overline{X})(Y_i - \overline{Y}))}{\sqrt{\sum_{i=1}^{n}(X_i - \overline{X})^2 \sum_{i=1}^{n}(Y_i - \overline{Y})^2}}, \tag{9}$$

where R_{xy} is the correlation between X and Y; X_i and Y_i are the values of variables at the i^{th} year; and $\overline{X}$ and $\overline{Y}$ are the annual values.

(4) Calculation of contribution rate

The effects of climate factors on NPP changes were analyzed by multiple regression analysis. The relative contribution rate of climate factors to NPP changes was also calculated. In order to determine the relative contribution rate of climate factors to NPP changes, we standardized the

data. Next, the regression equation of the standardized data sequence was obtained by regression analysis using the software SPSS. We calculated the contribution rate as follows:

$$Y_s=aX_{1s}+bX_{2s}+cX_{3s}\ldots, \tag{10}$$

$$\eta_1=\frac{|a|}{|a|+|b|+|c|+\ldots}, \tag{11}$$

where Y_s is the standardized value of a dependent variable; X_{1s}, X_{2s}, $X_{3s}\ldots$ are the standardized values of independent variables; η_1 is the contribution rate; and a, b and c are the regression coefficients of the regression equation of the standardized data sequence.

3 Results and discussion

3.1 Model calibration and uncertainty analysis

Verifying the accuracy of the model is a key challenge in NPP research (Gao et al., 2007). Two methods are usually used for the validation. The first approach is to compare the values between estimated NPP and observed NPP, while the second method applies comparison to validate the model by using former research production.

We show comparisons between the mean annual NPP during the period 2000–2014 from the CASA model and from observations at 18 sites across the Ili River Valley (Fig. 1a). In general, the CASA model performed fairly well in observed NPP, showing a correlation coefficient (R^2) of 0.65 (P<0.01), a root mean square error (RMSE) of 20.86 g C/(m^2•a), and precipitation of 61.04%. Overall, the good performance, as indicated by relatively high R^2 and lower RMSE and mean bias, suggests that the CASA model has a good potential to be used for estimating NPP in the Ili River Valley.

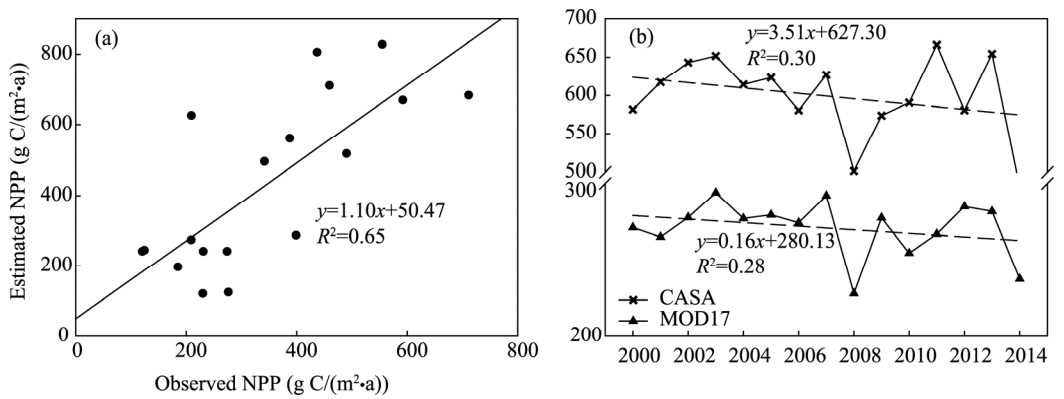

Fig. 1 Validation of the Carnegie-Ames-Stanford CASA model. (a) comparison between estimated net primary productivity (NPP) and observed NPP; (b) inter-annual variations of estimated NPP (CASA model) and MOD17 data.

In this paper, we compared and analyzed the spatial and temporal distribution pattern of NPP as estimated by CASA model and the MOD17 data (Fig. 1b). On the whole, the temporal and spatial distribution of the CASA model agrees well with the MOD17 data. By comparing the inter-annual variation trend of the two estimation results (Fig. 1b), we can see that the changing trend of the two estimated results is accordant. The rate of the NPP estimated by the CASA model was –3.51g C/(m^2•a), while it was –1.16 g C/(m^2•a) by the MOD17 data. The largest discrepancy between the two methods is that the estimated results of the CASA model were higher than those of the MOD17 data, which was consistent with previous research (Lei et al., 2014). Many researchers found that MOD17 products underestimated the productivity of the bush, grassland, and desert, but fit very well to temperate and broad leaf forest (Turner et al., 2005). This result emphasizes the importance of the data source and model mechanism in estimating vegetation NPP.

3.2 Spatial pattern of NPP

The spatial pattern of mean annual NPP during the period 2010–2014 is shown in Figures 2a and

b, representing that NPP distribution differs among different zones. Overall, annual NPP of the Ili River Valley was 599.19 g C/(m^2•a). In the southeastern and eastern Ili River Valley, NPP was higher than in its southern fringe and the whole valley. Annual NPP was generally higher than 1000 g C/(m^2•a) in large expanses of the eastern and southeastern Ili River Basin while being lower than 200 g C/(m^2•a) in the Ili River Valley and its southern fringe.

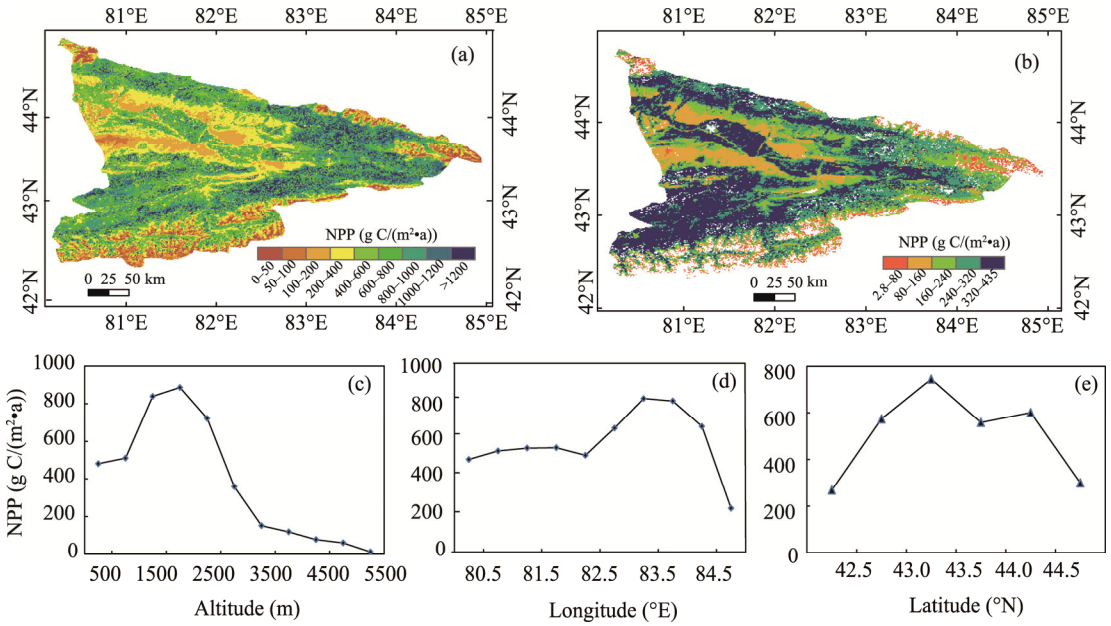

Fig. 2 Spatial distributions of mean annual net primary productivity (NPP) estimated by CASA model (a) and BIOME-BGC model (b). Changes in NPP along with altitude (c), longitude (d), and latitude (e).

Furthermore, by analyzing vegetation NPP at different altitudes in the study area, we can see that annual NPP varied according to altitude (Fig. 2c). Annual NPP ranged from 400 to 600 g C/(m^2•a) at low altitude, whereas it was generally higher than 800 g C/(m^2•a) at middle to high altitudes (about 2000 m), where productive mountain meadow and steppe meadow are extensively distributed. For altitudes above 3000 m, simulated NPP showed the gradients decreasing as the altitude increases. The annual NPP was generally about 50 g C/(m^2•a) in the southern fringe of the Ili River Valley.

Longitudinally, changes in NPP remained relatively stable in west of 82.5°E, being a value of about 500 g C/(m^2•a) (Fig. 2d). In areas located between 82.0°E and 85.0°E, the simulated NPP trend was "increasing-steady-decreasing" as the longitude increases. The maximum value was 850 g C/(m^2•a) in the areas stretching from 83.5°E to 84.0°E. According to latitude, annual NPP trends prove to be significantly different, showing a "decreasing-increasing" trend in areas located south of 43.7°N and an "increasing-decreasing" trend in areas located north of 43.7°N (Fig. 2e).

The changing trends of the two sides of the valley may be related to the changes of hydrothermal conditions as well as land cover changes from the valley to the top of the mountains (Yu et al., 2009). Topographic factors play an important role to the vegetation growth by affecting the reallocation of the hydrothermal combination (Du et al., 2018). In the mountains, the precipitation showed earlier increase and later decreases trend and the temperature gradually decreased with the increase in elevations. Therefore, in a certain elevation range, the hydrothermal conditions are suitable for vegetation growth. At high altitudes, the vegetation growth environment was poor due to the lower air temperature and less precipitation in the direction of longitude, the altitude of the Ili River Valley was gradually increasing as the longitude rises. In the latitude direction, the altitude of the Ili River Valley showed earlier increase and later decreases trend. That is why the spatial pattern of vegetation NPP had a close relationship with the elevation in Figure 2.

3.3 Temporal variations of NPP

The inter-annual variation in total terrestrial NPP over the Ili River Valley from 2000 to 2014 is shown in Figure 3. The NPP in the Ili River Valley experienced a slight decreasing trend from 2000 to 2014, with an annual decrease rate of –3.51 g C/(m^2•a). The mean annual NPP was about 581.5 g C/(m^2•a) in 2000 and 481.1 g C/(m^2•a) in 2014, and its declining percent was 1.15%. However, annual NPP trends for different elevation zones were significantly different (Fig. 3d). Specifically, annual NPP experienced a slight increasing trend in areas below 1000 m and above 3000 m, while the NPP rate in the low-altitude valley (6.34 g C/(m^2•a)) was higher than that in the high-altitude mountain (2.19 g C/(m^2•a)). This may be related to the human activity of sloping cropland reclamation.

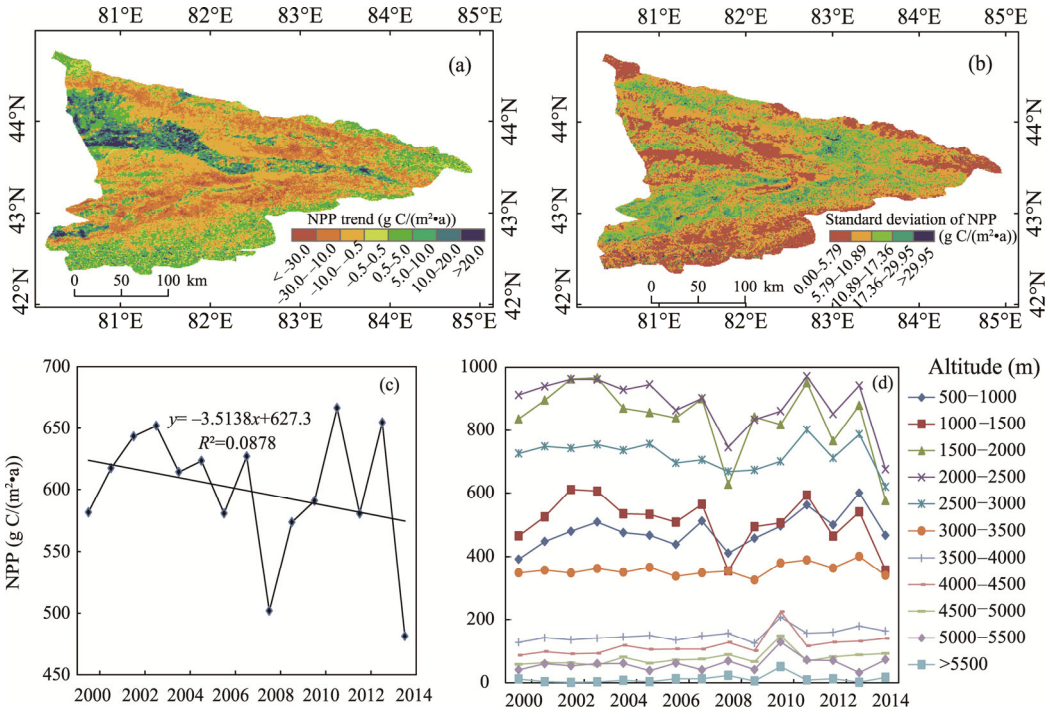

Fig. 3 Temporal variation of net primary productivity (NPP) in the Ili River Valley from 2000 to 2014. (a) NPP trends from 2000 to 2014; (b) standard deviation of NPP; (c) inter-annual variations of mean annual NPP; and (d) inter-annual variations of mean annual NPP at different altitudes.

The annual NPP in areas with altitudes ranging from 1000 to 3000 m showed a decreasing trend (Fig. 3d). The decrease of annual NPP in altitude ranging from 1500 to 2000 m (12.5 g C/(m^2•a)) was greater than in altitude ranging from 2000 to 2500 m (9.63 g C/(m^2•a)). In areas featuring altitude from 2500 to 3000 m, the decreasing trend appeared to slow, being an annual decrease rate of only 2.77 g C/(m^2•a).

According to our calculations, vegetation NPP in 55.69% of the areas showed a decreasing tendency, while 12.60% of the areas remained relatively stable and 31.71% appeared an increasing tendency. Vegetation NPP indicated an increasing trend in both high-altitude areas with low vegetation ratio and in low-altitude areas. In middle elevation zones on both sides of the valley, NPP showed a decreasing trend.

In analyzing the stability of NPP variations (Fig. 3b), we can see that it differed across regions. As a whole, NPP was stable in the Ili River Valley, showing the greatest stability in the low-altitude valley and high-altitude areas with the low vegetation ratio, which accounted for 48% of the study area. Fluctuation was mainly distributed at altitudes from 1000 to 3000 m on both sides of the valley. High fluctuation, which accounted for only 12%, was mainly scattered across central Nilka County, the Kalajun grassland, and the Narat grassland.

Using MATLAB, we analyzed the NPP inter-annual variation trends for different types of vegetation (Fig. 4). The change trends of most vegetation types were consistent with NPP trends for the entire study area. Except for water body and wetland, and unused land types, the annual NPP indicated a decreasing trend. The change rates differed across vegetation types, with the largest decreasing trend found in forest (at a rate of 4.79 g C/(m^2•a)), followed by grassland (at a rate of 4.64 g C/(m^2•a)), shrub (at a rate of 4.25 g C/(m^2•a)) and farmland (at a rate of 1.92 g C/(m^2•a)). As shown in Figures 4a and b, the vegetation NPP of sloping cropland significantly increased and the standard deviation was small, which means the changes of the vegetation NPP of sloping cropland were stable. The presumed main reason for these phenomena was that human activities have depressed the effects of natural factors. With the development of the agro-technological level and the disaster resistance ability of human, discover of mechanization, high-quality seeds, better techniques of irrigation and pest control have weakened the impact of natural factors on crop productivity.

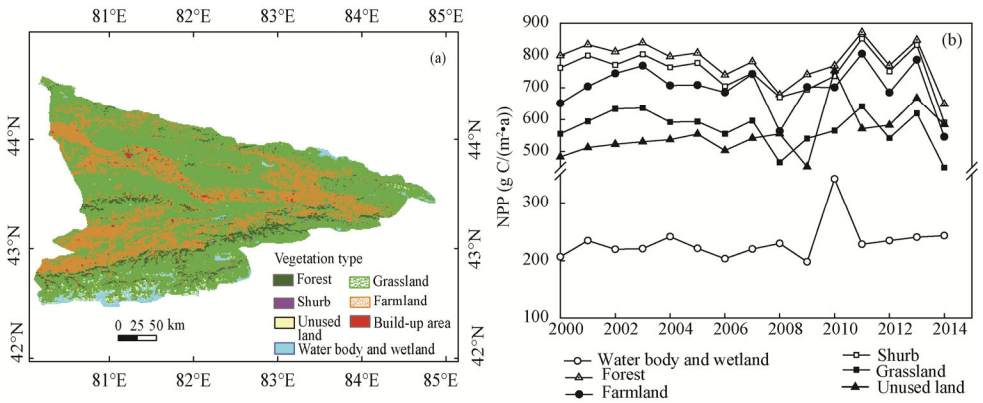

Fig. 4 Vegetation type (a) and inter-annual trends in net primary productivity (NPP) in different biomes (b) over the Ili River Valley from 2000 to 2014

3.4 Controlling factors for NPP variations

In order to understand the relationship between environmental change and vegetation NPP, scholars have found that temperature, precipitation, and solar radiation are the main climatic factors affecting the growth of terrestrial vegetation (Nemani et al., 2003; Zhao et al., 2010). In our study, regions that featured water resources as a major limiting factor accounted for 40% of the total vegetation coverage, while regions with temperature as the main control factor accounted for 33% and those with solar radiation accounted for 27% (Nemani et al., 2003).

By performing a comparative analysis of temperature, precipitation, and net radiation data from the past 15 years (Fig. 5), we can draw the conclusion that NPP in the Ili River Valley was sensitive to climate change. In fact, NPP had a significant positive correlation and a consistent trend with precipitation, while there was no obvious or only a weak correlation with temperature and solar net radiation. Vegetation NPP and annual accumulated precipitation revealed a positive correlation in 90.18% of the study area that was mainly distributed in the medium-high altitudes of the Ili River Valley. The remaining 9.82% of the vegetated land in the Ili River Valley showed a negative correlation between NPP and precipitation and was primarily situated in high-altitude mountain areas and low-altitude valley areas. A weak positive correlation appeared in the lower valley regions, including the southern Yining and in high-altitude areas such as northern Nilka County, Zhaosu County, and southern Tekes County, accounting for 29.65% of the total area. A negative correlation appeared on both sides of most parts of the middle elevation region in the Ili River Valley, accounting for 70.35% of the total area. A weak positive correlation between NPP and solar net radiation appeared in the high-altitude areas of the basin as well as in the low altitude areas of the valley, accounting for 26.91% of the total area. The weak negative correlation

distributed on both sides of most parts of the middle elevation region in the valley accounted for 73.09% of the total area.

The results of multiple linear regressions indicate the contribution rate of precipitation was the highest (69.26%), followed by net radiation (28.42%), while temperature had the lowest contribution rate (2.33%). These data clearly indicate that precipitation was the main limiting factor for NPP.

It is worth noting that the change in NPP was not continuous throughout the 15-year period (Fig. 5d), but instead showed a downward trend up to 2008 and a slope of –7.40 g C/(m^2•a). At higher temperature levels, the NPP significantly decreased along with the decreased precipitation up to 2008. After 2008, however, the NPP showed an increasing trend, with increasing precipitation and a slope of 3.21 g C/(m^2•a), except for 2014, when the NPP abruptly decreased due to the sharp increases in temperature and the reductions in precipitation.

In recent years, the annual precipitation of the study area ranged from 100 to 400 mm and experienced significant fluctuations. Furthermore, the annual mean temperature was 10.4°C and varied with altitude. Under such hydrothermal conditions, the NPP would rise in proportion to increases in precipitation, while the increases in temperature and radiation would accelerate the process of soil moisture loss (Jobbagy et al., 2002; Chen et al., 2014), thus limiting the growth of vegetation (Chen et al., 2012; Li et al., 2012; Yang et al., 2014).

The total annual amount of NPP on both natural and artificial vegetation was also compared and analyzed from 2000 to 2014 (Fig. 5e). We can see that the slope (at a rate of –0.190 g C/(m^2•a)) of total NPP for natural vegetation was notably higher than that for artificial vegetation (at a rate of –0.028 g C/(m^2•a)). The reason of this result is that agricultural technologies depress the climate effects on artificial vegetation (Li et al., 2014). Moreover, according to the Xinjiang Statistical Yearbook Data from 2010 to 2014, the crop area shows a rising trend and an increased rate of 92.4 km^2/a (Statistic Bureau of Xinjiang Uygur Autonomous Region, 2010–2014).

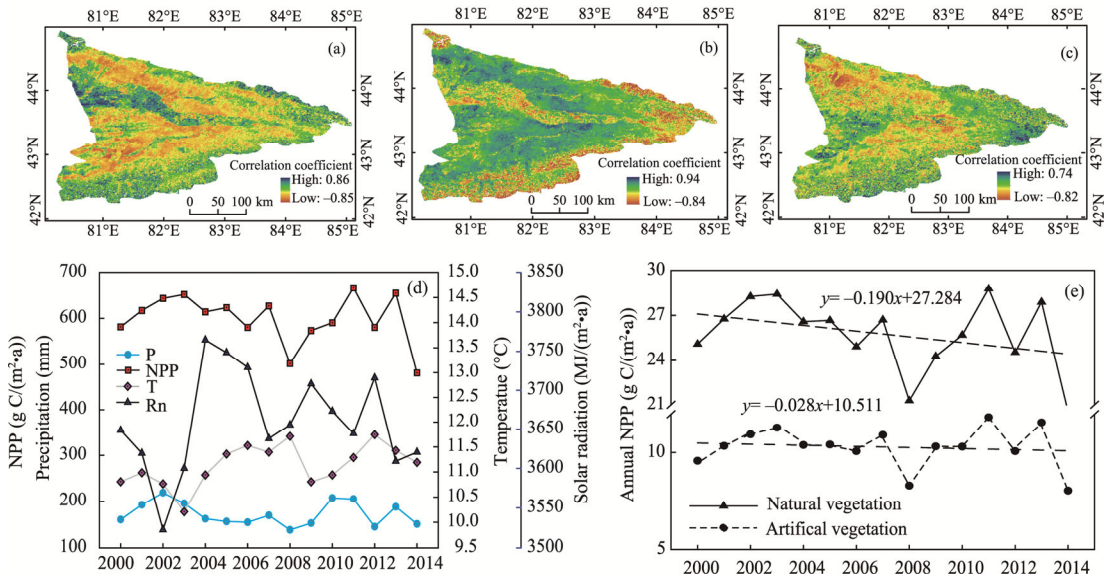

Fig. 5 Spatial distribution of correlation coefficients between annual net primary productivity (NPP) and temperature (a), precipitation (b), and net radiation (c). Trend analysis of climate factors from 2000 to 2014 (d). Inter-annual variations of annual NPP in artificial vegetation and natural vegetation across the Ili River Valley from 2000 to 2014 (e).

4 Conclusions

For the Ili River Valley, the spatio-temporal pattern of NPP and their relationship with climate

from 2000 to 2014 were analyzed using the CASA model in combination with climatic factors. We found that the CASA model performed well in the study area. Validation results showed that CASA could explain 61.04% of variation in observed NPP and the RMSE was 20.86 g C/(m^2•a). Temporally, the annual NPP of the Ili River Valley was 599.19 g C/(m^2•a), and showed a decreasing trend during the entire study period. Spatially, its distribution was affected by the vertical zonality of the valley. The annual NPP experienced a modest increasing trend in areas situated below 1000 m and above 3000 m, while annual NPP in areas situated between 1000 and 3000 m showed a decreasing trend. Our calculations revealed that vegetation NPP in 55.69% of the areas appeared to decrease, while 12.60% of the areas remained relatively stable and 31.71% showed increasing tendencies. Precipitation was found to be the dominant climatic factor that controlled the distribution of vegetation NPP in the study area and the correlations between NPP and climate factors differed along the vertical zones. Vegetation NPP and annual accumulated precipitation experienced a positive correlation in 90.18% of the area, with NPP trending higher in years with greater precipitation. A comprehensive understanding of the combined environmental control on ecosystem productivity remains a great challenge for further studies.

Acknowledgements

The research was supported by the Strategic Priority Research Program of the Chinese Academy of Sciences (XDA19030204), and the West Light Program of Chinese Academy of Sciences (2015-XBQN-B-17).

References

Chen A J, Xiao J D, Cao M L. 2016. Research on change of vegetation index and response to climate in Ili River valley based on MODIS data. Prataculture Science, 33(8): 1502–1508. (in Chinese)

Chen Y N, Yang Q, Luo Y, et al. 2012. Ponder on the issues of water resources in the arid region of northwest China. Arid Land Geography, 35(1): 1–9. (in Chinese)

Chen Y N, Li Z, Fan Y T, et al. 2014. Research progress on the impact of climate change on water resources in the arid region of Northwest China. Acta Geographica Sinica, 69(9): 1295–1304. (in Chinese)

Chen Z S, Chen Y N, Li W H, et al. 2010. Evaluating effect of land use change on environment in Ili valley based on ecosystem service value analysis. Journal of Desert Research, 30(4): 870–877. (in Chinese)

Chen Z S, Chen Y N, Chen Y P, et al. 2012. Response of ecological water requirement to land use change in the newly reclaimed area of Ili River basin in Xinjiang. Journal of Desert Research, 32(2): 551–557. (in Chinese)

Cui L L, Shi J, Xiao F J. 2018. Impacts of climatic factors and El Niño/La Niña events on the changes of terrestrial ecosystem NPP in China. Acta Geographic Sinica, 73(1): 54–66. (in Chinese)

Du M J, Zheng J h, Ren X, et al. 2018. Effects of topography on the distribution pattern of net primary productivity of grassland in Changji Prefecture, Xinjiang. Acta Ecological Sinica, 38(13): 1–11. (in Chinese)

Fan Y J, Hou X Y, Shi H X, et al. 2012. Effect of carbon cycling in grassland ecosystems on climate warming. Axta Prataculture Sinica, 21(3): 294–302. (in Chinese)

Feng Y M, Yao A D, Jiang L. 2014. Improving the CASA model and applying it to estimate the net primary productivity of arid region ecology system. Journal of Arid Land Resources and Environment, 28(8): 39–43. (in Chinese)

Field C B, Randerson J T, Malmstrom C M. 1995. Global net primary production: Combining ecology and remote sensing. Remote Sensing of Environment, 51(1): 74–88.

Gang C C, Wang Z Q, Zhou W, et al. 2015. Projecting the dynamics of terrestrial net primary productivity in response to future climate change under the RCP2.6 scenario. Environmental Earth Sciences, 74(7): 5949–5959.

Gao Q Z, Wan Y F, Li Y. 2007. Grassland net primary productivity and its spatiotemporal distribution in Northern Tibet: A study with CASA model. Chinese Journal of Applied Ecology, 18(11): 2526–2532. (in Chinese)

Hatfield J L, Asrar G, Kanemasu E T. 1984. Intercepted photosynthetically active radiation estimated by spectral reflectance. Remote Sensing of Environment, 14: 65–75.

He C Y, Liu Z F, Xu M, et al. 2017. Urban expansion brought stress to food security in China: evidence from decreased cropland net primary productivity. Science of the Total Environment, 576: 660–670.

Jobbagy E G, Sala O E, Paruelo J M. 2002. Patterns and controls of primary production in the Patagonian steppe: a remote

sensing approach. Ecology, 83(2): 307–319.

Lei H M, Huang M Y, Leung L R, et al. 2014. Sensitivity of global terrestrial gross primary production to hydrologic states simulated by the Community Land Model using two runoff parameterizations. Journal of Advances in Modeling Earth Systems, 6(3): 658–679.

Li D L, Yang J, Li W H, et al. 2016. Evaluating the sensitivity of soil erosion in the Yili River valley based on GIS and USLE. Chinese Journal of Ecology, 35(4): 942–951. (in Chinese)

Li P F, Sun X M, Zhao X Y. 2012. Analysis of precipitation and potential evapotranspiration in arid and semi-arid area of China in recent 50 years. Journal of Arid Land Resources and Environment, 26(7): 57–63. (in Chinese)

Li X, Zhu Z, Zeng H, et al. 2016. Estimation of gross primary production in China (1982–2010) with multiple ecosystem models. Ecological Modelling, 324: 33–44.

Li Y L, Pan X Z, Wang C K, et al. 2014. Changes of vegetation net primary productivity and its driving factors from 2000 to 2011 in Guangxi, China. Acta Ecologica Sinica, 34(18): 5220–5228. (in Chinese)

Li Z, Chen Y N, Wang Y, et al. 2016. Dynamic changes in terrestrial net primary production and their effects on evapotranspiration. Hydrology and Earth System Sciences, 20(6): 2169–2178.

Li Z S, Liu G H, Fu B J, et al. 2011. The potential influence of seasonal climate variables on the net primary production of forests in eastern China. Environment Management, 48 (6): 1173–1181.

Liang W, Yang Y, Fan D, et al. 2015. Analysis of spatial and temporal patterns of net primary production and their climate controls in China from 1982 to 2010. Agricultural and Forest Meteorology, 204: 22–36.

Mu S J, Li J L, Yang H F. 2013. Spatio-temporal variation analysis of grassland net primary productivity and its relationship with climate over the past 10 years in Inner Mongolia. Acta Prataculture Sinica, 22(3): 6–15. (in Chinese)

Nemani R R, Keeling C D, Hashimoto H. 2003. Climate-driven increases in global terrestrial net primary production from 1982 to 1999. Science, 300(5625): 1560–1563.

Pan S F, Tian H Q, Dangal S R S, et al. 2015. Impacts of climate variability and extremes on global net primary production in the first decade of the 21st century. Journal of Geographical Sciences, 25(9): 1027–1044.

Piao S L, Ciais P, Lomas M, et al. 2011. Contribution of climate change and rising CO_2 to terrestrial carbon balance in East Asia: A multi-model analysis. Global and Planetary Change, 75(3–4): 133–142.

Potter C S, Randerson J T, Field C B, et al. 1993. Terrestrial ecosystem production: A process model based on global satellite and surface data. Global Biogeochemical Cycles, 7(4): 811–841.

Ruimy A, Saugier B, Dedieu G. 1994. Methodology for the estimation of terrestrial net primary production from remotely sensed data. Journal of Geophysical Research, 97(D3): 5263–5283.

Statistic Bureau of Xinjiang Uygur Autonomous Region. 2010–2014. Xinjiang Statistical Yearbook. [2017-05-21]. http://www.xjtj.gov.cn/sjcx/tjnj_3415/. (in Chinese)

Sun G J, Li W H, Zhu C G, et al. 2016. Spatial variation analysis of topsoil bulk density in the Yili Valley, Xinjiang. Resources Science, 38(7): 1222–1228. (in Chinese)

Sun H L, Li W H, Chen Y P, et al. 2010. Response of ecological services value to land use change in the Ili River basin Xinjiang, China. Acta Ecologica Sinica, 30(4): 887–894. (in Chinese)

Tang C J, Fu X Y, Jiang D, et al. 2014. Simulating spatiotemporal dynamics of Sichuan grassland net primary productivity using the CASA model and *in situ* observations. The Scientific World Journal, 14(10): 1–12.

Turner D P, Ritts W D, Cohen W B, et al. 2005. Site-level evaluation of satellite-based global terrestrial gross primary production and net primary production monitoring. Global Change Biology, 11(4): 666–684.

Wang D L, Liu W P, Huang X Y. 2013. Trend analysis in vegetation cover in Beijing based on Sen+Mann-Kendall method. Computer Engineering and Applications, 49(5): 13–17. (in Chinese)

Wang X S, Hu Z W, Zhao W J. 2011. An integrated classification of grassland in large-scale based on MODIS EVI and multi-source data. Prataculture Science, 28(1):10–17. (in Chinese)

Yan J J, Qiao M, Zhou H F. 2013. Vegetation dynamics in Ili River valley of Xinjiang based on MODIS/NDVI. Arid Land Geography, 36(3): 512–519. (in Chinese)

Yang Y H, Chen Y N, Li W H, et al. 2010. Distribution of soil organic carbon under different vegetation zones in the Ili River Valley, Xinjiang. Journal of Geographical Sciences, 20(5): 729–740.

Yang Y T, Long D, Guan H D, et al. 2014. GRACE satellite observed hydrological controls on interannual and seasonal variability in surface greenness over mainland Australia. Journal of Geophysical Research: Biogeosciences, 119(12): 2245–2260.

Yu D Y, Shao H B, Shi P J, et al. 2009. How does the conversion of land cover to urban use affect net primary productivity? A

case study in Shenzhen city, China. Agricultural and Forest Meteorology, 149(11): 2054–2060.

Zhang F, Zhou G S, Wang Y H. 2008. Dynamics simulation of net primary productivity by a satellite data-driven CASA model in inner Mongolian typical steppe, China. Journal of Plant Ecology, 32(4): 786–797. (in Chinese)

Zhang W, Wang X H, Shen J X, et al. 2012. Spatial-temporal differentiation rule and sustainable development of oasis agricultural eco-economic system: a case study of Yili prefecture, China. Economic Geography, 32(4): 136–142. (in Chinese)

Zhang Y L, Wei Q, Zhou C P, et al. 2013. Spatial and temporal variability in the net primary production (NPP) of alpine grassland on Tibetan Plateau from 1982 to 2009. Acta Geographica Sinica, 68(9): 1197–1211. (in Chinese)

Zhao M, Running S W. 2010. Drought-induced reduction in global terrestrial net primary production from 2000 through 2009. Science, 329(5994): 940–943.

Zhou L L, Zhu H Z, Zhong H P, et al. 2016. Spatial analysis of soil bulk density in Yili, Xinjiang Uygur Autonomous Region, China. Acta Prataculture Sinica, 25(1): 64–75. (in Chinese)

Zhou W, Gang C C, Li J L, et al. 2014. Spatial-temporal dynamics of grassland coverage and its response to climate change in China during 1982–2010. Acta Geographica Sinica, 69(1): 15–30. (in Chinese)

Zhu W Q, Pan Y H, Long Z H, et al. 2005. Estimating net primary productivity of terrestrial vegetation based on GIS and RS: A case study in Inner Mongolia, China. Journal of Remote Sensing, 9(3): 300–307. (in Chinese)

Zhu W Q, Pan Y H, Hao H, et al. 2006. Simulation of maximum light use efficiency for some typical vegetation types in China. Chinese Science Bulletin, 51(4): 457–463.

Zhu W Q, Pan Y Z, Zhang J S. 2007. Estimation of net primary productivity of Chinese terrestrial vegetation based on remote sensing. Journal of Plant Ecology, 31(3): 413–424. (in Chinese)